Viscous merging of three vortices

Dam, Marc John Bordier; Hansen, Jesper Schmidt; Andersen, Morten

Viscous merging of three vortices

Marc J.B. Dam [a], Jesper S. Hansen [a,b], Morten Andersen [a,*]

[a] *IMFUFA, Roskilde University, Universitetsvej 1, 4000 Roskilde, Denmark*
[b] *Research Centre Glass and Time*

ARTICLE INFO

ABSTRACT

Localizing critical points of the vorticity of saddle and center type along with vorticity contours through saddle points provide a way to systematically investigate vorticity dynamics in two-dimensional viscous flow. Following this approach we investigate vortex interaction and merging using extremal points of the vorticity as a vortex identifier. Three Gaussian vortices with same strength are initially placed equidistantly and the vorticity contours of the flow is assessed as time progresses. Two transitions in the flow are observed for $Re \leq 400$ - a triangle bifurcation and three simultaneous cusp bifurcations. The core-growth model is shown to approximate well the vorticity transport equation in this case, providing quantitative and qualitative insights in the merging process, allowing for an analytical expression of the position of critical points of vorticity and a simple analytical expression for the triangle bifurcation observed in the flow.

1. Introduction

Interaction and merging of vortices play a central role in fluid dynamics. Merging of two vortices has been studied with an experimental approach as well as based on simulation of Navier–Stokes equation or simplified models such as two-dimensional inviscid vortex patch dynamics using contour methods, see the review by Leweke et al. [1]. Understanding the dynamics of few interacting vortices is instructive for investigating more complicated flows. Merging of three vortices is less frequent and relatively unexplored compared to merging of two vortices. We investigate the merging process of three vortices in unbounded two-dimensional viscous flow governed by the vorticity transport equation

$$\partial_t \omega = -\mathbf{u} \cdot \nabla \omega + \nu \Delta \omega, \tag{1}$$

where ω is the vorticity, $\mathbf{u} = (u_1, u_2)$ is the fluid velocity and ν is the kinematic viscosity of the fluid.

Describing vortex creation, interactions and merging hinge on an unambiguous definition of a vortex and plenty of definitions have been proposed [2]. In viscous flow, a natural generalization of a point vortex is an extremal point of the vorticity, leading to investigation of critical points of the vorticity satisfying

$$\partial_x \omega = \partial_y \omega = 0. \tag{2}$$

To classify a critical point of the vorticity the second order derivatives are useful, conveniently collected in the Hessian matrix, H.

With the determinant of the Hessian, $|H|$, being

$$|H| = (\partial_{xx}\omega)(\partial_{yy}\omega) - (\partial_{xy}\omega)^2, \tag{3}$$

the critical point is a saddle if $|H| < 0$ and an extremum if $|H| > 0$ (maximum if $\partial_{xx}\omega < 0$). *We identify a vortex as being an extremum of vorticity.* Carefully tracking critical points of the vorticity when varying system parameters provide a systematic way to investigate vortex formation, interaction and destruction during flow progression. To assess the qualitative change of the vorticity contours (i.e. level sets of the vorticity), the contours connected to the saddle points are essential. We apply this method as a post processing algorithm after numerically integrating Eq. (1) and compare to analytical predictions from a low dimensional model, *the core-growth model*, described below. With three equal, thin Gaussian vortices placed equidistantly initially, a vorticity minimum appears in the center of the vortex triangle i.e. a fourth counter rotating vortex. Hence, the current study could also be described as merging of four vortices.

Low dimensional models of vortex motion may provide analytical insight in fluid motion by applying methodology from various mathematical disciplines [3]. Point vortex motion applies to the early stage of vortex motion with concentrated vorticity as initial condition. The study of inviscid point vortex dynamics dates back to Helmholtz [4]. The motion of two point vortices is simple, the distance between them is preserved regardless of vortex strengths. Three point vortices show more complicated dynamics though it can still be analyzed in detail and is integrable [5]. Viscous effects are not included in the point vortex model. With a single point vortex as initial condition, the

* Corresponding author.
E-mail address: moan@ruc.dk (M. Andersen).

Lamb–Oseen vortex is an exact solution to the vorticity transport equation and the velocity field is given by

$$\frac{\overline{dz}}{dt} = \frac{\Gamma}{2\pi i}\frac{1}{z}\left(1 - \exp\left(-\frac{|z|^2}{4\nu t}\right)\right), \tag{4}$$

where ν is the viscosity, Γ is the vortex strength, $z = x + iy$ and $\overline{z}$ is the complex conjugate of z. The corresponding vorticity, ω, is given by

$$\omega = \frac{\Gamma}{4\pi \nu t}\exp\left(-\frac{|z|^2}{4\nu t}\right). \tag{5}$$

All integrable non zero initial vorticity evolved by the Navier–Stokes equation on the unbounded plane leads to a single, Gaussian vortex for long times [6] which shows the inadequacy of the point vortex model for long times where viscous effects matter. The studied initial condition here is a superposition of three concentrated Lamb–Oseen vortices with identical strengths, initially located equidistantly i.e. at the corners of an equilateral triangle.

The core-growth model (see [7]) constituted by equations ((6), (7), (8)) below describes how each Gaussian vortex is being pulled around in the plane by the remaining Gaussian vortices, and simultaneously each Gaussian vortex core is spreading out due to viscosity. Each vortex is affected by the velocity field of the other $N-1$ vortices and thus the velocity of Gaussian vortex j located at position z_j is given by

$$\frac{\overline{dz_j}}{dt} = \sum_{k \neq j}^{N}\frac{\Gamma_k}{2\pi i}\frac{1}{z_j(t) - z_k(t)}\left(1 - \exp\left(-\frac{|z_j(t) - z_k(t)|^2}{4\nu t}\right)\right), \tag{6}$$

where Γ_k is the vortex strength of vortex k. The velocity field at any point in the plane is the sum of contributions from each Gaussian vortex

$$\frac{\overline{dz}}{dt} = \sum_{k=1}^{N}\frac{\Gamma_k}{2\pi i}\frac{1}{z - z_k(t)}\left(1 - \exp\left(-\frac{|z - z_k(t)|^2}{4\nu t}\right)\right). \tag{7}$$

The corresponding vorticity in the core-growth model is

$$\omega = \sum_{k=1}^{N}\frac{\Gamma_k}{4\pi \nu t}\exp\left(-\frac{|z - z_k(t)|^2}{4\nu t}\right), \tag{8}$$

with initial conditions being N point vortices

$$\omega(z, 0) = \sum_{k=1}^{N}\Gamma_k\delta(z - z_k(0)). \tag{9}$$

We will use the notation that the *Gaussian vortices* are centered at z_k. We obtain analytical insight in the merging process from the core-growth model which is shown to approximate well the vorticity transport equation for moderate Reynolds number. Note, the core-growth model will not in general provide an exact solution to the Navier–Stokes equation, yet provides accurate predictions and is useful in understanding vortex dynamics.

If one neglected the exponential term in Eq. (6) we would arrive at the well known point vortex equations and since these have been subject to much study a few remarks are in place. First, the core-growth model is non autonomous in contrast to the point vortex equations. Second, steady state solutions of the point vortex equations are equivalent to the roots of a polynomial, for the core-growth model exponential terms are also present. Third, for the core-growth model, the vorticity is not just a sum of Dirac delta distributions, in fact even for fixed Gaussian vortex positions the topology of the vorticity may show interesting dynamics owing to the explicit time dependence. Hence, the core-growth model is more complicated to analyze which is the price for the

inclusion of viscous effects which are non existing in the point vortex model.

Few previous studies have addressed the core-growth model. Three, initially aligned Gaussian vortices are investigated by Jing et al. [7]. Due to the selected initial vortex positions and vortex strengths, the Gaussian vortices remain aligned but rotate according to the core-growth model which is verified from simulating the vorticity transport equation. Evolving the configuration using the point vortex equation, the configuration is stationary, hence the rotation in the core-growth model is viscously induced. Jing et al. [8] investigate two core-growth vortices, one symmetric and one asymmetric case providing insight in the passive tracer evolution during merging. Kim & Sohn [9] analyze the core-growth model with three vortices focusing on self similar motion and show that the Gaussian vortex centers cannot collapse in finite time contrary to the point vortex model [10]. Andersen et al. [11] investigate the topology of the vorticity based on the core-growth model for two vortices with arbitrary strengths. The merging time predicted in the core-growth model is shown to match numerical solutions of the Navier–Stokes equation at low Reynolds numbers. The intermediate topologies of the vorticity in the merging process, as well as the transitions (bifurcations) leading to merging, are identified from the core-growth model and found to match those from the vorticity transport equation. Nielsen et al. [12] rely on the Q-criterion as vortex identifier and investigate the core-growth model with two vortices. Experiments show that initiating two vortices by rotating plates in a fluid leads to an initial Gaussian profile for each vortex, hence advocates for the use the core-growth model also for non vanishing initial core size [13].

Considering time and Reynolds number as bifurcation parameters we investigate the vorticity topologies with three Gaussian vortices with equal strength placed equidistantly as initial conditions. We examine the evolving vorticity topologies from simulation of the vorticity transport equation and analytically using the core-growth model.

2. Analysis of the core-growth model

We consider three, equidistant, point vortices with same strengths, Γ, as initial condition, (Eq. (9)), i.e.

$$z_1(0) = r_0, \quad z_2(0) = r_0\exp\left(\frac{2\pi}{3}i\right), \quad z_3(0) = r_0\exp\left(\frac{4\pi}{3}i\right). \tag{10}$$

Evolving according to the core-growth model Eq. (6), the Gaussian vortices remain on an equilateral triangle for all future time, in particular

$$z_k(t) = z_k(0)\exp\left(i\phi(t)\right), \tag{11}$$

with

$$\phi(t) = \frac{\Gamma}{2\pi r_0^2}\left(t - \int_0^t \exp\left(-\frac{3r_0^2}{4\nu\tilde{t}}\right)d\tilde{t}\right), \tag{12}$$

where the integral can be computed numerically to machine precision in e.g. Matlab using the exponential integral function. The validity of Eq. (11) and Eq. (12) is easily seen by inserting in Eq. (6) to see it satisfied. Thus, the Gaussian vortex centers rotate around the origin with decaying speed. Substituting Eqs. (11) and (12) in (8), the vorticity is

$$\omega(z) = \frac{\Gamma}{4\pi \nu t}\sum_{k=1}^{3}\exp\left(-\frac{|z - z_k(0)e^{i\phi(t)}|^2}{4\nu t}\right). \tag{13}$$

Consider rotating coordinates z_r defined by

$$z_r(t) = ze^{-i\phi(t)}, \tag{14}$$

then Eq. (13) simplifies to

$$\omega(z_r) = \frac{\Gamma}{4\pi \nu t} \sum_{k=1}^{3} \exp\left(-\frac{|z_r - z_k(0)|^2}{4\nu t}\right). \tag{15}$$

In the co-rotating coordinate system, the Gaussian vortex centers are fixed at their initial positions given by Eq. (10).

The rotation angle $\phi(t)$ (Eq. (12)) and the vorticity (Eq. (15)) increase linearly with Γ. A linear scaling of the vorticity has no impact vorticity contour topology i.e. the location of the critical points of vorticity. The effect of increasing viscosity is a slowdown of the rotation $\phi(t)$. For the vorticity, ν and t only enters as the product νt. Therefore, an increasing ν impacts like an increase in time. As we will investigate the vorticity contours for all $t > 0$, then for increasing ν no new vorticity contour patterns will emerge, only the transition between different patterns will happen faster.

The number of free parameters in the model is reduced by introducing the dimensionless time $\tau = r_0^{-2} 4\nu t$, the dimensionless vorticity $\tilde{\omega} = \Gamma^{-1}\pi r_0^2 \omega$ and the dimensionless position $\tilde{z} = r_0^{-1} z_r$. For convenience the tilde is then skipped such that $\tilde{z}$ is renamed to z etc. In these units the vorticity simplifies to

$$\omega(z) = \frac{1}{\tau} \sum_{k=1}^{3} \exp\left(-\frac{|z - e^{\frac{2k\pi}{3}i}|^2}{\tau}\right). \tag{16}$$

The study of critical points (recall Eq. (2)) of Eq. (16) with τ as bifurcation parameter is the focus in the remaining section. The rotation rate of the three Gaussian vortices is proportional to Γ. Hence, for the core-growth model, increasing Γ increases the speed of rotation but does not alter the patterns of the vorticity. Rotational symmetry of $\frac{2}{3}\pi$ rotation around the origin is ensured if $\omega(z) = \omega\left(e^{\frac{2\pi i}{3}}z\right)$. By direct computation this property is verified

$$\omega\left(e^{\frac{2\pi i}{3}}z\right) = \frac{1}{\tau} \sum_{k=1}^{3} \exp\left(-\frac{|e^{\frac{2\pi i}{3}}z - e^{\frac{2\pi i}{3}k}|^2}{\tau}\right)$$

$$= \frac{1}{\tau} \sum_{k=1}^{3} \exp\left(-\frac{|z - e^{\frac{2\pi i}{3}(k-1)}|^2}{\tau}\right) = \omega(z). \tag{17}$$

Rotational symmetry with any integer times $\frac{2}{3}\pi$ follows similarly. Reflection symmetry around $y = 0$ is guaranteed if $\omega(\bar{z}) = \omega(z)$ which is easily verified using $|z|^2 = |\bar{z}|^2$ for any complex number, z.

$$\omega(z) = \frac{1}{\tau} \sum_{k=1}^{3} \exp\left(-\frac{|\bar{z} - e^{-\frac{2\pi i}{3}k}|^2}{\tau}\right)$$

$$= \frac{1}{\tau} \sum_{k=1}^{3} \exp\left(-\frac{|\bar{z} - e^{\frac{2\pi i}{3}k}|^2}{\tau}\right) = \omega(\bar{z}) \tag{18}$$

The reflection symmetry around the remaining two axis of symmetry are ensured by a combination of the rotation symmetry and the reflection symmetry around $y = 0$.

We proceed using Cartesian coordinates. Explicitly, $x_1 = x_2 = -\frac{1}{2}$, $x_3 = 1$, and $y_1 = -y_2 = \frac{\sqrt{3}}{2}$, $y_3 = 0$.

$$\omega = \frac{1}{\tau} \sum_{k=1}^{3} \exp\left(-\frac{(x - x_k)^2 + (y - y_k)^2}{\tau}\right) \tag{19}$$

The first derivatives of the vorticity is given by

$$\partial_x\omega = -\frac{2}{\tau^2} \sum_{k=1}^{3} (x - x_k)\exp\left(-\frac{(x - x_k)^2 + (y - y_k)^2}{\tau}\right) \tag{20}$$

and

$$\partial_y\omega = -\frac{2}{\tau^2} \sum_{k=1}^{3} (y - y_k)\exp\left(-\frac{(x - x_k)^2 + (y - y_k)^2}{\tau}\right). \tag{21}$$

For $x \leq -\frac{1}{2}$ the terms in Eq. (20) are non-negative and one is strictly positive hence $\partial_x\omega > 0$. From symmetry we can conclude that all critical points of the vorticity are within the triangle spanned by the three Gaussian vortices. To proceed we start by investigating $(0,0)$ as the exponential terms here are all equal. It is easily seen that $\partial_x\omega(0,0) = \partial_y\omega(0,0) = 0$ i.e. the origin is a critical point of the vorticity for any positive τ. The second derivatives of the vorticity are needed to calculate $|H|$ (recall Eq. (3))

$$\partial_{xx}\omega = -\frac{2}{\tau^2} \sum_{k=1}^{3} \left(1 - \frac{2}{\tau}(x - x_k)^2\right)\exp\left(-\frac{(x - x_k)^2 + (y - y_k)^2}{\tau}\right), \tag{22}$$

$$\partial_{yy}\omega = -\frac{2}{\tau^2} \sum_{k=1}^{3} \left(1 - \frac{2}{\tau}(y - y_k)^2\right)\exp\left(-\frac{(x - x_k)^2 + (y - y_k)^2}{\tau}\right), \tag{23}$$

and

$$\partial_{xy}\omega = \frac{4}{\tau^3} \sum_{k=1}^{3} (x - x_k)(y - y_k)\exp\left(-\frac{(x - x_k)^2 + (y - y_k)^2}{\tau}\right). \tag{24}$$

The mixed derivative vanish at the origin, $\partial_{xy}\omega(0,0) = 0$, and

$$\partial_{xx}\omega(0,0) = \partial_{yy}\omega(0,0) = 6\tau^{-3}\exp\left(-\tau^{-1}\right)(1 - \tau). \tag{25}$$

$|H|$ is the square of the right hand side of this equation. This implies that for any positive τ with $\tau \neq 1$, there is a vortex at the origin. For $0 < \tau < 1$ this vortex is a minimum of the vorticity, and for $\tau > 1$ the vortex is a maximum of the vorticity. To characterize this transition, the third order Taylor polynomial, $p_\tau(x,y)$, of the vorticity around $(0,0)$ for any $\tau > 0$ is useful. Systematic use of Taylor expansions to locally characterize flow patterns is well established [14,15]. The difference between $\omega(x,y)$ and $p_\tau(x,y)$ depends on fourth order terms, hence $p_\tau(x,y)$ is a good approximation for $\omega(x,y)$ near $(0,0)$.

$$p_\tau(x,y) = e^{-\frac{1}{\tau}}\tau^{-4}\left(3\tau^3 - 3(\tau - 1)\tau x^2 - 3(\tau - 1)\tau y^2 + x^3 - 3xy^2\right), \tag{26}$$

which for $\tau = 1$ reduce to

$$p_1(x,y) = e^{-1}\left(3 + x^3 - 3xy^2\right). \tag{27}$$

For $\tau = 1$ level curves trough the origin must satisfy $p_1(x,y) = 3e^{-1}$ so $x = 0$ or $y = \pm\frac{\sqrt{3}}{3}x$. Hence, for $\tau = 1$ the origin is a degenerate saddle having six branches with any two neighboring branches being separated by an angle of $\frac{\pi}{3}$.

As expected, the symmetry of ω is also present in the third order approximation, i.e. reflection symmetry and rotations with multiples of $\frac{2\pi}{3}$. There are three critical points of Eq. (26), located at $(\mathcal{X}_1, \mathcal{Y}_1) = 2\tau(\tau - 1)(1,0)$ and by symmetry $(\mathcal{X}_2, \mathcal{Y}_2) = 2\tau(\tau - 1)\left(-\frac{1}{2}, \frac{\sqrt{3}}{2}\right)$, $(\mathcal{X}_3, \mathcal{Y}_3) = 2\tau(\tau - 1)\left(-\frac{1}{2}, -\frac{\sqrt{3}}{2}\right)$. The critical points are located at the lines of reflection symmetry and cross the origin at $\tau = 1$. The Hessian at any of the critical points of Eq. (26) is $-108 \cdot e^{-\frac{2}{\tau}}\tau^{-6}(\tau - 1)^2$ which guarantees that the critical points away from the origin are saddles for $\tau \neq 1$. As p_τ has the same value at the three saddles, they are expected to be heteroclinically connected. We now investigate this conjecture.
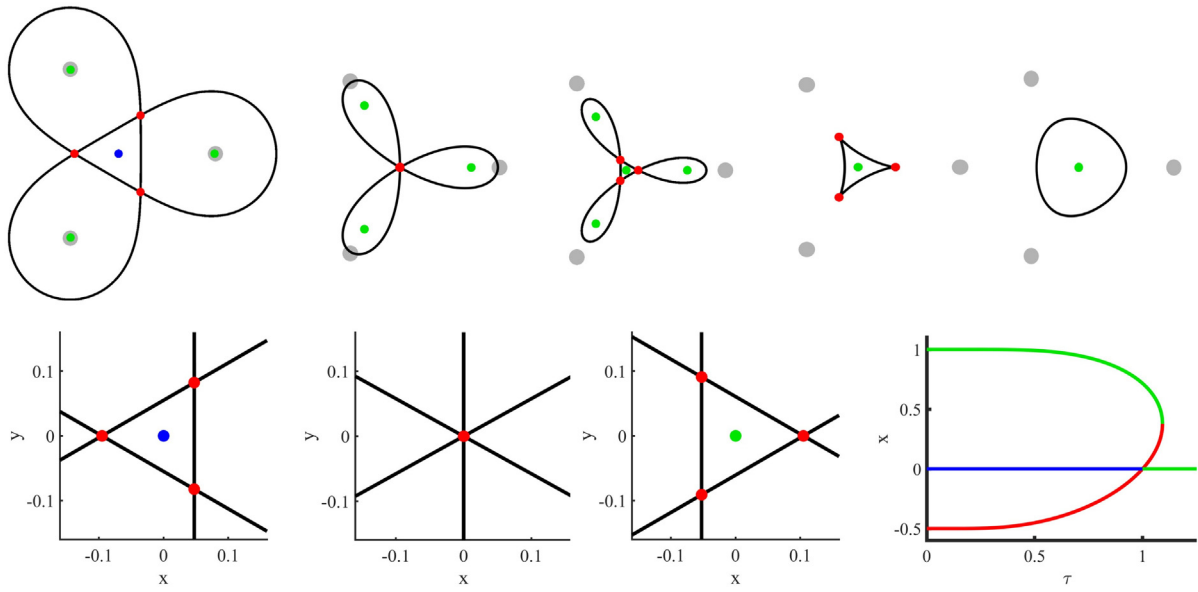
Fig. 1. The vorticity topologies of the core-growth model with three, equidistant point vortices as initial condition shown in the corotating frame where the Gaussian vortices have fixed positions. The organizing vorticity level curve through the saddle points is included when it exists (four first panels). Red dots are saddle points, green dots are vortices (maxima), blue dots are vortices (minima), gray dots are the Gaussian vortices, placed equidistantly on the unit circle. From left to right τ values are 0.49, 1.00, 1.05, 1.09, 1.70. Bottom row, the triangle bifurcation: The first three panels show $p_\tau(x, y)$ at τ values 0.95, 1, 1.05. The last panel shows the critical points of vorticity for $y = 0$.

First, notice that $p_\tau(x, y) = p_\tau(\mathcal{X}_1, \mathcal{Y}_1)$ may be solved for y^2 as

$$y^2(x) = \frac{4\tau^3 (\tau - 1)^3 - 3\tau (\tau - 1) x^2 + x^3}{3\tau (\tau - 1) + 3x}, \tag{28}$$

which is valid for $x \neq -\tau (\tau - 1)$ and simplifies to a straight line since the denominator divides the numerator

$$y_\pm(x) = \pm \frac{\sqrt{3}}{3} (x - 2\tau (\tau - 1)) . \tag{29}$$

For x tending to $-\tau (\tau - 1)$, $y_+(x)$ tend to $\mathcal{Y}_2$ and as $p_\tau (\mathcal{X}_1, \mathcal{Y}_1) = p_\tau (\mathcal{X}_2, \mathcal{Y}_2)$, y_+ is a continuous level curve of the vorticity joining the two saddle points $(\mathcal{X}_1, \mathcal{Y}_1)$ and $(\mathcal{X}_2, \mathcal{Y}_2)$.

Similarly $(\mathcal{X}_1, \mathcal{Y}_1)$ and $(\mathcal{X}_3, \mathcal{Y}_3)$ are on the same level curve, and by symmetry $(\mathcal{X}_2, \mathcal{Y}_3)$ and $(\mathcal{X}_3, \mathcal{Y}_3)$ are joined by a vorticity contour being a straight line given by $(-\tau(\tau - 1), y)$. Hence, for $\tau \neq 1$, there is a vortex at $(0, 0)$ surrounded by a vorticity contour formed as an equilateral triangle, with saddle points at the corners. At $\tau = 1$ the triangle is collapsed, and for $\tau > 1$, the vortex at the origin is again surrounded by an equilateral triangular vorticity contour with saddle points at the corners, only the shape has been reflected in the y - axis compared to τ smaller than 1. We coin this a *triangle bifurcation* which is illustrated in Fig. 1. Restricting the attention to lowest order nontrivial terms in the Taylor approximation, here of order three, is justified by the bifurcation being local − for τ sufficiently close to 1, the critical points of vorticity are close to $(0,0)$ and hence we may skip higher order terms. The corners of the triangle i.e. the saddle points of the vorticity are characterized by identical values of vorticity due to rotation symmetry in the core-growth model as well as in the vorticity transport equation. Therefore, it is not a peculiarity of the third order approximation that the saddle points are connected by a vorticity contour. The main consequence of the third order approximation is that these contours are straight line segments and not bending.

The investigation of critical points of the vorticity is extended to the line $y = 0$ not necessarily close to the origin. As $\partial_y \omega(x, 0) = 0$ a detailed analysis is possible, keeping in mind that we only need to investigate $-\frac{1}{2} < x < 1$, $x \neq 0$. Requiring $\partial_x \omega(x, 0) = 0$ allows for isolating τ in Eq. (20)

$$\tau = \frac{3x}{\log \left(\frac{2x+1}{1-x} \right)} . \tag{30}$$

The above formula is convenient for numerically computing critical points of vorticity, see Fig. 1, though a formula isolating for x instead of τ would be desirable for analytical investigation.

By numerically solving $\frac{d\tau}{dx} = 0$ to find $x = 0.37720$, and substitute this value in Eq. (30) we can compute the merging time, τ_m, to be 1.09. Critical points of the vorticity are located at the origin and two branches approaching 1 and $-\frac{1}{2}$ for τ tending to zero, and the two branches are merging at $\tau = \tau_m$ leaving only the vortex at the origin. The second order derivatives of the vorticity are used to classify the critical points via the $|H|$ - value at these points to obtain: *The merging time is $\tau = 1.09$, where the three saddles and vortices at the lines of symmetry merge a distance 0.38 from the origin leaving only the vortex at $(0, 0)$.* In the last panel of Fig. 1 this is the cusp bifurcation with upper branch being the green curve and lower branch being the red curve.

It is left to consider potential critical points of vorticity off the lines of symmetry. Consider polar coordinates (r, θ) and let $\phi_1 = 0$, $\phi_2 = \frac{2\pi}{3}$, and $\phi_3 = \frac{4\pi}{3}$, then

$$\partial_\theta \omega = -2 \frac{r}{\tau} \exp \left(-\frac{1 + r^2}{\tau} \right) \sum_{k=1}^{3} \sin(\theta - \phi_k) \exp \left(2 \frac{r}{\tau} \cos(\theta - \phi_k) \right) . \tag{31}$$

We want to solve $\partial_\theta \omega = 0$ for all $r > 0$ and $\tau > 0$ which is facilitated by r and τ only occur in the fraction $\frac{r}{\tau}$. Numerically solving Eq. (31) for the two variables θ and $\frac{r}{\tau}$ only allows solutions corresponding to the three axes of reflection i.e $\theta = \phi_k$ i.e. there are no critical points of vorticity off the symmetry lines.
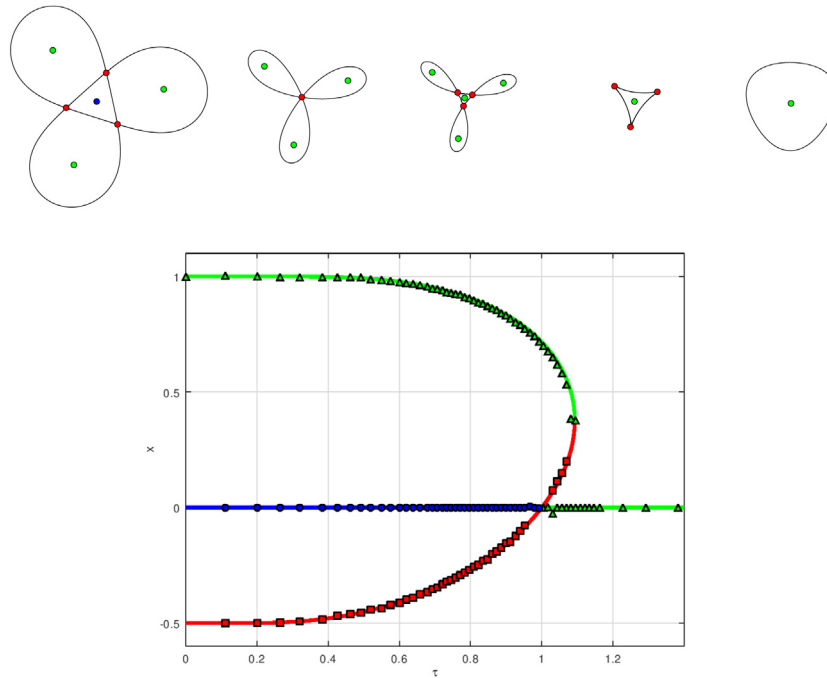
Fig. 2. Simulation of the vorticity transport equation at $Re = 10$. The top row shows the five distinct vorticity contour patterns, corresponding to τ being 0.49, 1.00, 1.05, 1.09, 1.70. The lower figure shows location and type of the critical points of vorticity for the core-growth model (color) and the vorticity transport equation (triangles are maxima, circles are minima and squares are saddles) with excellent agreement. Red dots are saddle points, green dots are vortices (maxima), blue dots are vortices (minima).

In summary, the core-growth model has three distinct topologies as time evolves, and two transitions (bifurcations), independent of Γ. At $\tau = 1$ the vortex at the origin transforms from a vortex minimum to a vortex maximum trough a transition which we denote a triangle bifurcation. At $\tau = 1.09$ the three outer vortices at the lines of symmetry disappear through cusp bifurcations leaving a single vortex at the origin.

3. Numerical solution of the vorticity transport equation

To examine the validity of the core-growth model the underlying fluid dynamics equations are solved. This involves simultaneously solving the vorticity transport equation, Eq. (1), the Poisson equation for the stream function, $\Delta\psi = -\omega$, and $\partial_x\psi = -u_2$, $\partial_y\psi = u_1$. We use a Runge–Kutta fourth order scheme with adaptive time step for the solution of the vorticity transport equation, along with a spectral method using the fast Fourier transform for the solution of Poisson's equation for the stream function. The Runge–Kutta implementation is based on the algorithm presented in [16] with standard spatial finite difference schemes. The individual time derivatives are approximated by forward differences and the spatial derivatives are approximated by second order central differences. The simulations are done with periodic boundary conditions showing no measurable boundary effect when the length of computational domain is doubled.

The error, used for the adaptive time step algorithm, is estimated by comparing the Runge–Kutta fourth order scheme with a 2-step Runge–Kutta fourth order scheme with half the time step. The error estimator is

$$err = \frac{\max\{|\omega_{1-step} - \omega_{2-step}|\}}{\max\{\omega_{1-step}\}}, \tag{32}$$

where the maxima are taken over the entire simulation domain. We have chosen the simulation domain to be $[0, 12] \times [0, 12]$ with a grid size of 512 points in each dimension. This means the

grid spacing is $\Delta x \approx 0.023$. The maximal error per time step is set to 0.01%. For the initial condition, the Gaussian vortices are placed equally spaced on a circle with center $(6, 6)$. The initial condition is given by Eq. (8). To minimize the numerical errors we do not initialize the vorticity from a Dirac delta, but from a diffused system corresponding to $t_0 = \frac{(\Delta x)^2}{4\nu}$. Applying this initial condition results in a relative difference of less than 0.1% between the analytical Lamb–Oseen vortex dynamics and the numerics; the error estimator is the same maximum error as Eq. (32).

The Reynolds number is defined as $Re = \Gamma/\nu$. When simulating at different Reynolds numbers, we keep the vortex strengths Γ fixed and change the viscosity ν. To test for finite size effects, we ran two simulations with three identical vortices at $Re = 10$: One with a simulation domain as above and one with a simulation domain of $[0, 24] \times [0, 24]$ with the same grid spacing. We then ran post-processing to determine the trajectories of the critical points on the x-axis in both cases. Within uncertainties of the post-processing method we see no difference in the trajectories between the two cases and thus conclude that the simulation domain is large enough to ignore finite size effects.

4. Numerical results and discussion

Fig. 2 shows simulation of the vorticity transport equation for $Re = 10$. For $\tau < 1$ there are seven critical points all located on the axes of symmetry: One minimum at the center of vorticity, three maxima close to the core-growth vortex centers and three saddle points in between the maxima. At $\tau = 1$ the saddle points bifurcate at the center of vorticity, which for $\tau > 1$ is a maximum. The saddle points pass through the center of vorticity and bifurcate with the maxima for $\tau = 1.09$, after which only the maximum at the center of vorticity remains. The simulations are in good agreement with the core-growth model as the same vorticity patterns occur and the transitions between the vorticity patterns occur at the same time as in the core-growth model. In particular, the triangle bifurcation at the origin
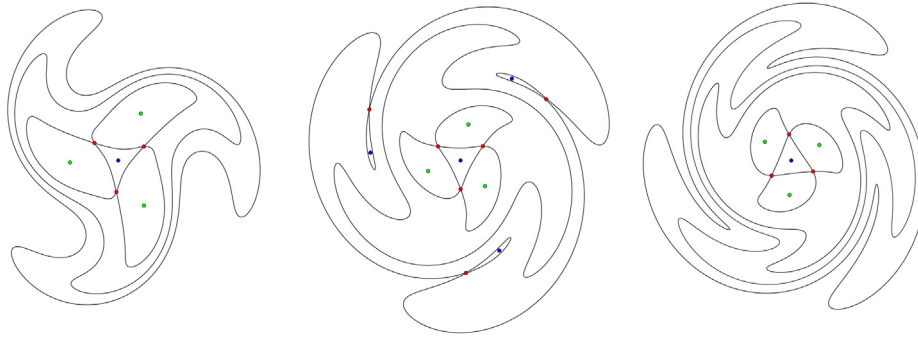
Fig. 3. Vorticity topologies at $Re = 500$ for τ being 0.26, 0.34, 0.37 reveal a topology not included in the core-growth model (middle panel). Three outer vortices are created simultaneously through a cusp bifurcation with saddles being on the same vorticity contour. The outer vortices disappear again through a cusp bifurcation. For later times the topologies are the same as shown in Fig. 2.

is observed for the vorticity transport equation as well as in the core-growth model. The small deviations between the core-growth model and the vorticity transport equations for τ near 1 and 1.09 are due to post-processing difficulties of locating the critical points when they are very close to a bifurcation point. For increasing Re the vortex merging time of the vorticity transport equation decreases with the vorticity patterns and transitions being unaltered i.e. identical to the core-growth model. At Re between 400 and 450 a new pattern emerges, three new vortices are created through cusp bifurcations outside the existing vortex structures, preserving rotational symmetry by $\frac{2\pi}{3}$, see Fig. 3. The new vortices arise as a shear layer is formed. The new vortices vanish soon after creation through a cusp bifurcation. Closer to the center of vorticity, the vorticity transport equation and the core-growth model have matching topologies, and the transitions in the core-growth model are also present in the vorticity transport equation for $Re > 400$.

At large Reynolds number, instabilities lead to nonlinear convective merging [17]. Meunier et al. [18] describe the merging via different stages where convective merging is critical as the vortex cores exceed a threshold value. For the lower Reynolds numbers and the special initial positions investigated here, this effect is less prominent which is essential for the applicability of the core-growth model, since the conserved distance between the Gaussian vortex positions imply the merging is driven by diffusion of vorticity rather than convective merging. From the merging time $\tau_m = 1.09$ and the definition of τ we obtain the relation in unscaled time as

$$t_m = 1.09 \frac{r_0^2}{4\Gamma} Re \, , \tag{33}$$

i.e. a linear relation between merging time and Re underpinning viscous merging. The merging of two symmetric vortices is simpler than merging of three vortices as it is characterized by a pitchfork bifurcation where two vortices and a saddle point collapse at the merging time, after which only a single vortex is left at the center of vorticity [11]. In this study a relation similar to Eq. (33) was derived and verified for low Re.

Studying the patterns and transitions of the vorticity contours relies on locating the critical points of vorticity, both extrema and saddle points, which may be applied as a post processing algorithm of numerical solutions to the vorticity transport equation. For some cases, analytical insight may be gained via the core-growth model to obtain a complete description of the vorticity pattern and transitions which seem to hold for moderate Re. We expect the core-growth model to be useful for studying vortex interactions and merging for other flows with few vortices with various strengths and initial positions.

Declaration of competing interest

The authors declare that they have no known competing financial interests or personal relationships that could have appeared to influence the work reported in this paper.

Data availability

Data will be made available on request.

References

[1] T. Leweke, S.L. Dizes, C. Williamson, Dynamics and instabilities of vortex pairs, Annu. Rev. Fluid Mech. 48 (1) (2016) 507–541, http://dx.doi.org/10.1146/annurev-fluid-122414-034558.
[2] Y. Zhang, K. Liu, H. Xian, X. Du, A review of methods for vortex identification in hydroturbines, Renew. Sustain. Energy Rev. 81 (2018) 1269–1285, http://dx.doi.org/10.1016/j.rser.2017.05.058.
[3] H. Aref, Point vortex dynamics: a classical mathematics playground, J. Math. Phys. 48 (6) (2007) 065401.
[4] H. Helmholtz, Über integrale der hydrodynamischen gleichunm gen, J. Reine Angew. Math. 55 (1858) 25555.
[5] H. Aref, Motion of three vortices, Phys. Fluids 22 (3) (1979) 393–400.
[6] T. Gallay, C.E. Wayne, Global stability of vortex solutions of the two-dimensional Navier-Stokes equation, Comm. Math. Phys. 255 (1) (2005) 97–129.
[7] F. Jing, E. Kanso, P.K. Newton, Viscous evolution of point vortex equilibria: The collinear state, Phys. Fluids 22 (12) (2010) 123102.
[8] F. Jing, E. Kanso, P.K. Newton, Insights into symmetric and asymmetric vortex mergers using the core growth model, Phys. Fluids 24 (2012) 073101.
[9] S. Kim, S. Sohn, Interactions of three viscous point vortices, J. Phys. A 45 (45) (2012) 455501.
[10] H. Aref, Self-similar motion of three point vortices, Phys. Fluids 22 (5) (2010) 1–12, http://dx.doi.org/10.1063/1.3425649.
[11] M. Andersen, C. Schreck, J.S. Hansen, M. Brøns, Vorticity topology of vortex pair interactions at low Reynolds numbers, Eur. J. Mech. B 74 (2019) 58–67, http://dx.doi.org/10.1016/j.euromechflu.2018.10.022, URL http://www.sciencedirect.com/science/article/pii/S0997754618303170.
[12] A. Nielsen, M. Andersen, J. Hansen, M. Brøns, Topological bifurcations of vortex pair interactions, J. Fluid Mech. 917 (2021) http://dx.doi.org/10.1017/jfm.2021.191.
[13] P. Meunier, U. Ehrenstein, T. Leweke, M. Rossi, A merging criterion for two-dimensional co-rotating vortices, Phys. Fluids 2002 (2002) 2757–2766.
[14] M. Brøns, J.N. Hartnack, Streamline topologies near simple degenerate critical points in two-dimensional flow away from boundaries, Phys. Fluids 11 (2) (1999) 314–324, http://dx.doi.org/10.1063/1.869881.
[15] M. Brøns, Streamline topology: Patterns in fluid flows and their bifurcations, in: H. Aref, E. van der Giessen (Eds.), in: Advances in Applied Mechanics, vol. 41, Elsevier, 2007, pp. 1–42, http://dx.doi.org/10.1016/S0065-2156(07)41001-8, URL https://www.sciencedirect.com/science/article/pii/S0065215607410018.
[16] E. Weinan, J.-G. Liu, Vorticity boundary condition and related issues for finite difference schemes, J. Comput. Phys. 124 (2) (1996) 368–382.
[17] E.A. Overman, N.J. Zabusky, Evolution and merger of isolated vortex structures, Phys. Fluids 25 (8) (1982) 1297–1305.
[18] P. Meunier, S. Le Dizès, T. Leweke, Physics of vortex merging, C.R. Physique (2005) 431–450.